Applied Catalysis B: Environmental 91 (2009) 587–595

Contents lists available at ScienceDirect

Applied Catalysis B: Environmental

journal homepage: www.elsevier.com/locate/apcatb

Study of the selective catalytic reduction of NO_x on an efficient Fe/HBEA zeolite catalyst for heavy duty diesel engines

Peter Balle [a], Bastian Geiger [a], Dirk Klukowski [a], Matias Pignatelli [a], Stefan Wohnrau [a], Michael Menzel [b], Ingo Zirkwa [c], Gunther Brunklaus [d], Sven Kureti [a,*]

[a] Institut für Technische Chemie und Polymerchemie, Universität Karlsruhe, Karlsruhe Institute of Technology, D-76128 Karlsruhe, Germany
[b] Bundesanstalt für Materialforschung und -prüfung, D-12489 Berlin, Germany
[c] HJS Fahrzeugtechnik GmbH & Co KG, D-58706 Menden, Germany
[d] Max Planck Institut für Polymerforschung, Ackermannweg 10, D-55128 Mainz, Germany

ARTICLE INFO

Article history:
Received 6 May 2009
Received in revised form 24 June 2009
Accepted 27 June 2009
Available online 3 July 2009

Keywords:
SCR
BEA
Zeolite
Fe
Active sites
Diesel engine
Hydrothermal aging
SO_2 stability

ABSTRACT

The present paper addresses the removal of NO_x from the exhaust of heavy duty vehicles using the SCR technique. The studies were conducted with a highly active H-BEA zeolite exhibiting a molar Si/Al ratio of 12.5 and a Fe load of 1.0 wt.% (1Fe/HBEA). The pronounced efficiency of 1Fe/HBEA is reflected by the apparent turnover frequency being superior to traditional $V_2O_5/WO_3/TiO_2$. The nature of the Fe sites was investigated with high resolution transmission electron microscopy (HRTEM), ^{57}Fe Mössbauer spectroscopy and powder X-ray diffraction (PXRD). In connection with previous examinations it is deduced that the iron sites represent octahedrally coordinated high spin Fe^{3+} cations. Furthermore, highly dispersed species, which are the most active sites, are supposed to be paramagnetic, while oligomeric and particulate structures indicate superparamagnetic behaviour.

The practical evaluation of the 1Fe/HBEA catalyst was systematically carried out including laboratory studies of granulated powder and honeycomb samples as well as engine bench tests. For the latter studies a coated honeycomb prototype was employed showing very similar efficiency as referred to a commercial $V_2O_5/WO_3/TiO_2$ pattern.

Furthermore, 1Fe/HBEA exhibits pronounced hydrothermal stability after aging at 550 °C which represents an elevated exhaust temperature of heavy duty vehicles. The aging caused no change in fast SCR, i.e. when a $c(NO_2)/c(NO_x)$ ratio of 0.5 was used, and only minor decline in standard SCR. The slight aging effect is mainly referred to little decrease in BET surface area and NH_3 uptake, respectively. PXRD indicated maintenance of the BEA structure, whereas ^{27}Al nuclear magnetic resonance spectroscopy showed removal of some Al from the zeolite framework. Contrary, UV–vis spectroscopy evidenced no effect of hydrothermal aging on the composition of the Fe sites. Finally, the catalyst also maintained its efficiency after SO_2 aging at 300 °C. Diffuse reflectance infrared Fourier transform spectroscopic studies showed adsorption of molecular SO_2 on the zeolite substrate releasing already at about 400 °C.

1. Introduction

The selective catalytic reduction (SCR) of NO_x by NH_3 is a well-established process for the removal of nitrogen oxides from stationary power and waste combustion plants. In SCR, NO_x is catalytically reduced to yield N_2 and H_2O according to the so-called standard SCR reaction, i.e. $4NO + 4NH_3 + O_2 \rightarrow 4N_2 + 6H_2O$. The most common SCR catalyst used today is $V_2O_5/WO_3/TiO_2$ which is employed in the form of coated or homogeneous monoliths [1].

The SCR procedure is the only technique converting NO_x selectively into N_2 under strongly oxidising conditions. Thus, selective catalytic reduction has been considered as technology of choice when deNO_x became an issue for lean burn engines, particularly diesel engines. Indeed, SCR has advanced to a state-of-the-art technology for heavy duty vehicles in the last years. However, a constraint is the required storage of NH_3 which cannot be supplied from gas cylinders due to its toxicity. Hence, only harmless precursors releasing NH_3 by heating are applicable, whereas an aqueous solution of urea is currently favoured. This agent called "AdBlue" reveals an urea content of 32.5 wt.%.

The application of the SCR technology in vehicles results in a complex exhaust aftertreatment system. The primal design includes the oxidation of NO into NO_2 on the Pt pre-catalyst

* Corresponding author. Tel.: +49 721 608 8090; fax: +49 721 608 2816.
E-mail address: Kureti@ict.uni-karlsruhe.de (S. Kureti).

0926-3373/$ – see front matter © 2009 Elsevier B.V. All rights reserved.
doi:10.1016/j.apcatb.2009.06.031

(diesel oxidation catalyst, DOC) leading to drastic increase in SCR particularly below 250 °C (fast SCR, $2NO + 2NO_2 + 4NH_3 \rightarrow 4N_2 + 6H_2O$) [2,3]. However, in the designing of the DOC it has to be considered that molar NO_2/NO_x ratios above 0.5 can cause strong NH_4NO_3 deposits deactivating the SCR catalyst. The second unit contains the urea dosing system implying the urea hydrolysis catalyst, for instance alumina or titania. The subsequent part of the system involves the SCR catalyst followed by the NH_3 oxidation catalyst to avoid slip of NH_3.

A challenging feature of SCR is the limited high-temperature stability of the $V_2O_5/WO_3/TiO_2$ catalysts being unfavourable for the coupling of SCR with particulate filter systems in diesel passenger cars. In filter regeneration performed by post-injection of fuel, the temperature can increase up to approx. 800 °C [4] resulting in complete deactivation of the V_2O_5 catalyst. Contrary, this overheating of the SCR catalyst is currently not an issue for heavy duty vehicles, where soot is removed from the particulate filters by using the CRT technique (Continuously Regenerating Trap); note that for heavy duty and non-road applications an active regeneration could be relevant in future as well. CRT uses NO_2 to initiate the soot oxidation occurring between 220 and 450 °C [5]. Furthermore, in some countries the toxicological concern of vanadia catalysts is discussed controversially and therefore its substitution by harmless and thermally stable materials represents a current matter for lean burn applications. In this concern, ion-exchanged Fe-ZSM5 zeolites are presently the most-investigated materials [6–14], while Cu-ZSM5 [15], $CeO_2/WO_3/ZrO_2$ [16] and nano-sized Fe_2O_3/ZrO_2 [17] also show outstanding SCR performance. Additionally, we have recently reported in this journal on H-BEA zeolites modified by iron oxide which exhibit promising activity as well. A pronounced efficiency has been shown for the sample revealing a Fe content of 1.0 wt.% (1Fe/HBEA) [18]. Thus, the present article addresses the practical evaluation of this catalyst including both laboratory and engine bench tests with particular focus on heavy duty vehicles. Additionally, the hydrothermal and SO_2 aging of 1Fe/HBEA was investigated. As a supplement to our previous paper, the Fe sites were complementarily characterised by high resolution transmission electron microscopy, powder X-ray diffraction and ^{57}Fe Mössbauer spectroscopy.

2. Experimental

2.1. Preparation and characterisation of the catalyst

The 1Fe/HBEA catalyst was prepared by incipient wetness method as described in detail recently [18]. Briefly, H-BEA zeolite (Si/Al = 12.5, Sud-Chemie) was used as carrier being impregnated with a solution of $Fe(NO_3)_3$. The sample was finally calcined in air at 450 °C for 3 h. The load of Fe was confirmed by atom absorption spectrometry (AAS 4100, Perkin-Elmer). Moreover, the catalyst was characterised by using high resolution transmission electron micrography (HRTEM) and ^{57}Fe Mössbauer spectroscopy. The Mössbauer spectroscopic investigations employing the natural abundance of ^{57}Fe were performed at −196 °C and 20 °C. The analyses were conducted on a constant acceleration spectrometer, i.e. a commercial one from WissEl Electronics and a CM-2201 developed by the Institute for Analytical Instrumentation St. Petersburg. ^{57}Co implemented in chromium matrix was used as radiation source showing an average activity of about 1.5 GBq. Proportional counters (LND Inc.) were used with a voltage between 1800 V and 1950 V to collect the spectra. The sample (ca. 300 mg) was placed into the sealable cylindrical polyethylene compartment (i.d.: 19 mm). The Mössbauer spectra were recorded at a maximum velocity of +/−3.6 mm/s if no magnetic splitting was observed; otherwise the data were collected with a maximum velocity of +/−12.3 mm/s. For comparison purposes, an α-Fe_2O_3 sample was used; this reference was prepared by polyvinyl alcohol technique including final annealing at 650 °C as described recently [19]. All the spectra are referred to a α-Fe foil (Goodfellow).

Additionally, high resolution transmission electron micrographs (HRTEM) were taken with a Philips CM200 FEQ equipped with an EDX detector. For sample preparation, a dispersion with iso-propanol was made which was sprayed on a silicium coated grid by using ultrasound. After drying at ambient conditions, bright field HRTEM images were recorded at an acceleration voltage of 200 kV.

Powder X-ray diffraction analyses (PXRD) were performed at room temperature on a D 501 from Siemens with Ni filtered Cu K_α radiation. A 2θ step size of 0.02 was used with an integration time of 2 s.

To evaluate the 1Fe/HBEA catalyst under practical conditions two down-sized cordierite honeycombs were coated. For this purpose, pure H-BEA powder was ground in a ball mill to a median diameter of 5 μm and was subsequently modified by iron oxide as described above. With the use of this sample an aqueous slurry was prepared at a zeolite/H_2O mass ratio of 0.1. The cylindrical cordierite monolith (400 cpsi) was then dipped into this slurry several times until the targeted loading was achieved. After each dipping, the honeycomb was dried at 105 °C for 3 h. The scaling and loading of the prepared honeycomb systems is listed in Table 1.

2.2. SCR studies

The SCR studies were carried out on a laboratory as well as an engine test bench. The performance of the catalysts is presented in terms of conversion of NO_x ($X(NO_x) = c(NO_x)_{in} - c(NO_x)_{out}/c(NO_x)_{in}$) and NH_3 ($X(NH_3)$) as well as selectivity of N_2O ($S(N_2O) = 2c(N_2O)_{out}/c(NO_x)_{in} - c(NO_x)_{out}$).

2.2.1. Laboratory bench tests

The laboratory tests were performed by using a synthetic diesel model exhaust, whereas granulated powders as well as coated honeycombs were taken. Powder samples were pressed to pellet with a pressure of 40 MPa, granulated and sieved to a size of 125–250 μm to avoid discharge; it should be stated that pressing does not affect the BET surface area of the catalysts. The sample (200 mg) was packed into the quartz glass tube reactor (i.d.: 6 mm) and fixed with quartz wool. $V_2O_5/WO_3/TiO_2$ granules were used as reference taken from a commercially available homogeneous monolith. Before the measurement, the sample was pre-treated at 500 °C for 30 min under flowing N_2 to remove possible impurities and to obtain reproducible reaction conditions. After this, the feed was added at a total flow of 0.50 l/min (STP) resulting in a space velocity (S.V.) of 50,000/h. The feed was comprised of 500 ppm NO, 500 ppm NH_3, 5 vol.% O_2 and N_2 as balance, whereas 1000 ppm CO, 5 vol.% CO_2 and 5 vol.% H_2O were optionally present.

For the honeycomb system another quartz glass reactor (i.d.: 24 mm) was employed, while a realistic diesel model exhaust was taken consisting of 500 ppm NO, 500 ppm NH_3, 1000 ppm CO, 5 vol.% O_2, 4 vol.% CO_2, 4 vol.% H_2O and N_2 as balance. The total flow was 6.00 l/min (STP) corresponding to a S.V. of 35,000 h^{-1}. To evaluate the fast SCR activity a molar NO_2/NO_x ratio of 0.5 was

Table 1
Scaling and loading of the honeycombs coated by 1Fe/HBEA.[a].

Parameter	Laboratory sample	Engine sample
Length	28.5 mm	3.0 in.
Diameter	22.0 mm	2.0 in.
Loading	82 g/l	95 g/l

[a] Cell density of the cordierite honeycomb was 400 cpsi.

Table 2
Experimental parameters of the engine bench tests.[a].

T (°C)	S.V./1/h	$c(NO_x)$[b] (ppm)	$c(NO_2)/c(NO_x)$[c]
200	53,500	410	0.13
225	54,000	470	0.20
250	55,000	565	0.28
275	56,000	645	0.35
300	58,000	690	0.44
325	60,000	675	0.53
350	62,500	700	0.55
375	63,500	715	0.51
400	66,000	740	0.39
425	67,500	750	0.38
450	70,500	825	0.30

[a] $c(NH_3)/c(NO_x)$ was always 1.0.
[b] NO_x raw emission of the engine.
[c] NO_x production refers to the DOC activity, S.V. of DOC was between 100,000 and 150,000 1/h.

adjusted. For this purpose, NO_2 was obtained by NO oxidation on a Pt catalyst [18]. Prior to the experiment, the honeycomb was pre-treated as described for the granulated samples.

All gases (Air Liquide) were fed from independent mass flow controllers (MKS Instruments), while H_2O was produced by catalytic H_2 oxidation [18]. The stainless steel pipes of the bench were heated to 150 °C to prevent H_2O condensation as well as NH_4NO_3 formation. The temperature was recorded by two K-type thermocouples being directly placed in front of and behind the catalyst bed, respectively. The difference of inlet and outlet temperature was always below 10 K. In the experiments, the temperature was decreased in steps of 50 K from 500 to 150 °C and the reactor effluents were recorded after reaching steady state. The gas-phase analyses were carried out by a hot measuring FTIR spectrometer (MULTI-GAS Analyzer 2010, MKS Instruments).

2.2.2. Engine bench tests

For the tests in real exhaust a Liebherr diesel engine (934 s; 115 kW) equipped with a commercial diesel oxidation catalyst (DOC) was employed. Downstream to the DOC the AdBlue injection unit was located including an electronic steering system (JM/HJS), a liquid pump (UDS 2.5, Grundfos), nozzle (Fleetguard) and NO_x sensor (Smart-Sensor, Siemens/NGK). Finally, the catalytic honeycomb was positioned at tailpipe end, whereas the exhaust stream was split to evaluate the sample at realistic space velocities. NO_x and NH_3 was checked by a Horbia MEXA 1170 NX, while CO, CO_2, HC and O_2 was monitored with a Pierburg AMA 2000 system. Inlet and outlet temperature of the SCR catalyst was controlled by K-type thermocouples showing negligible differences; temperature was varied by changing the operation point of the engine thus simultaneously changing S.V., NO_x raw emission and NO_2/NO_x ratio (Table 2). The molar NH_3/NO_x ratio was always kept at 1 and the SCR data were recorded under steady-state conditions.

For reference purposes a commercial $V_2O_5/WO_3/TiO_2$ catalyst was used representing a coated full size cordierite honeycomb (400 cpsi, 2.5 l). This sample was investigated in the full exhaust stream under very similar conditions as demonstrated in Table 2.

2.3. Hydrothermal and SO_2 aging

Hydrothermal and SO_2 aging of the 1Fe/HBEA catalyst was performed on a laboratory bench being very similar to that mentioned in Section 2.2.1, whereas for each aging stage fresh granules (200 mg) were taken. In the hydrothermal exposure, the sample was treated for 24 h at 550 °C with a flow of 1.00 l/min (STP) consisting of 10 vol.% H_2O and 16 vol.% O_2 (N_2 balance); the adjusted temperature was representative for heavy duty vehicles. The Fe sites of the fresh and aged catalyst were examined by diffuse reflectance UV–vis spectroscopy (UV–vis) as described lately [18]. Furthermore, the BET surface area was checked using multi-point Sorptomatic 1990 (Porotec). The sample was pre-treated at 350 °C for 2 h in vacuum (10^{-4} mbar) and cooled to −196 °C, and then the N_2 isotherm was recorded. BET surface area was derived from adsorption data referring to p/p_0 ratios from 0.05 to 0.30. The structure of the zeolite was checked by PXRD (Section 2.1) as well as nuclear magnetic resonance spectroscopy (NMR). ^{27}Al MAS NMR and MQ MAS analyses were performed on a Bruker Avance-III 850 MHz (20 T) spectrometer operating at 221.56 MHz using a 2.5 mm MAS probe. Additional ^{27}Al MAS NMR spectra were acquired by a Bruker Avance 500 (11.7 T) spectrometer operating at 130.32 MHz, employing single pulse excitation at 42 kHz rf-field strength and pulse duration corresponding to $\pi/18$ pulse angle. In all cases, magic angle spinning was carried out at a rotation speed of 25 kHz. Chemical shifts are referenced relative to an aqueous $Al(NO_3)_3$ solution. ^{27}Al MQ MAS experiments were done using the two-pulse z-filtered procedure [20]. Both the excitation and reconversion pulse were optimised for maximum signal at 150 kHz rf-field, the relaxation delay was set to 1.5 s. Quadrature detection in the F1 dimension was achieved using STATES [21]. All MQ MAS spectra were sheared so that the F1 axis is the isotropic dimension and the F2 axis contains the second-order quadrupolar lineshape. ^{27}Al multiple quantum (MQ) MAS NMR was used to both determine the coordination of aluminium present in the samples and to monitor dealumination possibly taking place in the hydrothermal exposure [22]. In an MQ MAS experiment, the quadrupolar interaction was refocused and an isotropic direction free from anisotropic quadrupolar interactions is present in the spectra. Any broadening visible in the F1 dimension originates from chemical shift distributions, e.g. due to variations in the Al–O–Si bond angles or Al–O bond lengths, thus resulting in distributions of the quadrupolar coupling constants [23].

NH_3 storage capacity was investigated by temperature programmed desorption (TPD). In TPD, the sample (0.500 g) was pre-treated in N_2 flow at 500 °C for 15 min and was then cooled to 250 °C. At this temperature, the catalyst was exposed to a mixture of 500 ppm NH_3 in N_2. Subsequently, it was flushed and then TPD was started at a ramp of 10 K/min up to 600 °C using N_2 as carrier gas (500 ml/min, STP).

The sulphur aging was performed at 300 °C by exposing the catalyst for 48 h to a mixture of 10 ppm SO_2 and 10 vol.% O_2 at a total flow of 1.00 l/min (STP); N_2 was used as balance. Furthermore, the interaction of SO_2 with 1Fe/HBEA was investigated by diffuse reflectance infrared Fourier transform spectroscopy (DRIFTS) using a Nicolet 5700 equipped with a MCT detector and DRIFTS optics (all from Thermo Electron). The pure catalyst (ca. 10 mg) was heated in the IR cell to 500 °C for 15 min for conditioning purposes and was subsequently cooled to 300 or 50 °C; these steps were done under flowing N_2. After this, the material was exposed for several hours to a mixture of (a) 20 ppm SO_2 in N_2 or (b) 20 ppm SO_2, 10 vol.% O_2 and N_2 (balance) at a flow of 100 ml/min (STP). Sample spectra were collected in the SO_2 admission and after flushing with N_2 while accumulating 550 scans; the unreacted catalyst was taken as background implying same pre-treatment. Additionally, after SO_2 saturation at 50 °C and flushing with N_2, the sample was heated at 400 °C for 15 min in N_2 flow. Subsequently, it was cooled again to 50 °C and a spectrum was recorded. DRIFTS data are presented in form of $-\log R$ with $R = R_r/R_u$; R_r is the reflectance of the reacted and R_u that of the unreacted sample.

3. Results and discussion

3.1. Nature of the Fe sites of the 1Fe/HBEA catalyst

The HRTEM images of 1Fe/HBEA and the H-BEA reference are depicted in Fig. 1. For the 1Fe/HBEA sample HRTEM coupled with

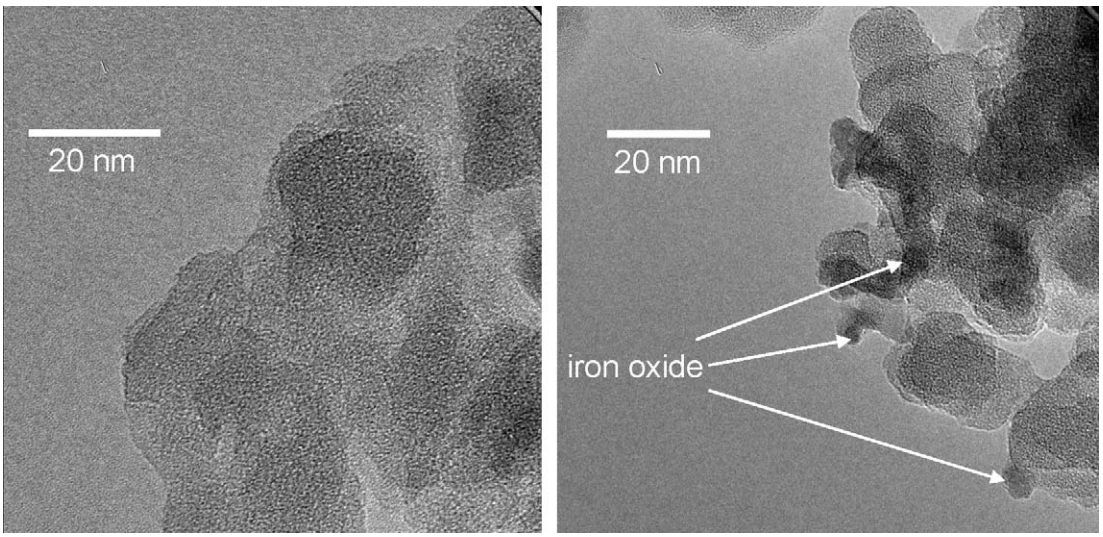

Fig. 1. HRTEM image of the bare H-BEA zeolite (left) and the 1Fe/HBEA catalyst (right).

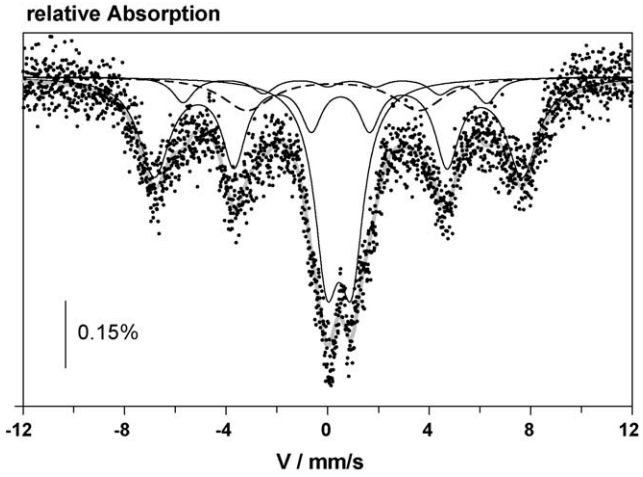

Fig. 2. ^{57}Fe Mössbauer spectrum of the 1Fe/HBEA zeolite catalyst recorded at −196 °C. The diagram includes the sub-bands obtained by deconvolution (black curves) as well as the trace arising from addition of these sub-bands (grey curve).

local EDX analysis showed iron oxide particles ranging from 2 to 5 nm. As the size of the BEA channels is 0.76 nm × 0.63 nm and 0.55 nm × 0.65 nm, it is obvious that these aggregates are localised on the external surface of the zeolite. With the use of UV–vis spectroscopy we have reported lately that the Fe oxo species are mainly in the form of oligomeric structures (ca. 59%), while highly dispersed sites implying isolated centres (ca. 25%) and particulate entities (ca. 16%) are present in minor abundance [18]. Considering these results we assign the iron oxide structures found by HRTEM to particulate species and possibly to large oligomers as well. Nevertheless, the micrograph of 1Fe/HBEA does not evidence Fe oxo entities being deposited on the internal surface. A deeper investigation by taking higher magnifications was not useful, as then the electron beam destroyed completely the zeolite structure. Thus, it is difficult to estimate the extent of the Fe species positioned on the internal and external surface. We explicitly do not exclude the presence of highly dispersed and oligomeric species on both locations which is supposed to be associated with the incipient wetness impregnation allowing the site-independent absorption of the $Fe(NO_3)_3$ solution. Moreover, we have previously reported that the Fe sites are present in the form of extra-framework species and they do not block the zeolite channels; the specific surface area of the BEA zeolite (ca. 560 m^2/g) is only affected at Fe loads exceeding 2 wt.%. Additionally, no signals were obtained in the PXRD pattern which might refer to iron oxide species (not depicted). This finding is consistent with the small size of the Fe aggregates identified by HRTEM and with the relatively low content of Fe. Diffraction reflexes relating to α-Fe_2O_3 were found at Fe loads above 2 wt.% only corresponding to particles up to the sub-μm range [18].

The ^{57}Fe Mössbauer spectrum of 1Fe/HBEA recorded at −196 °C is displayed in Fig. 2 indicating a sextet type signal. This spectrum was deconvoluted by using a minimum number of Lorentz curves leading to five sub-bands which describe the collected spectrum well (R^2 is 1.06). The obtained sub-bands represent two doublets and three sextets characterised in Table 3. It should be stated that the sextet sub-signal with an isomer shift of 0.54 mm/s contributes negligibly to the spectrum (ca. 1%), while the sextet pattern with 0.47 mm/s shows superimposition of its inner bands. The isomer shifts of all the sub-bands are between 0.44 and 0.57 mm/s thus being assigned to high spin Fe^{3+} cations with octahedral coordination. Other coordination polyhedrons as well as low spin Fe^{3+} and Fe^{2+} sites are rather excluded as they show clearly differing isomeric shifts [24]. The predominant presence of Fe in the oxidation state +3 is substantiated by our previous UV/VIS analyses [18,25]. The sextet sub-bands are associated with

Table 3
Results of the ^{57}Fe Mössbauer spectroscopic analysis of the 1Fe/HBEA catalyst performed at −196 °C.

Signal[a]	Isomer shift (mm/s)	Quadrupole split (mm/s)	Magnetic hyperfine field (T)	Fraction (%)
Doublet	0.47	0.79		20
Doublet	0.57	1.88		13
Sextet	0.55	−0.20	48.8	1
Sextet	0.47	−0.04	45.4	33
Sextet	0.44	−0.15	39.0	33

[a] Signals were obtained by deconvolution of the recorded spectrum; R^2 is 1.06.

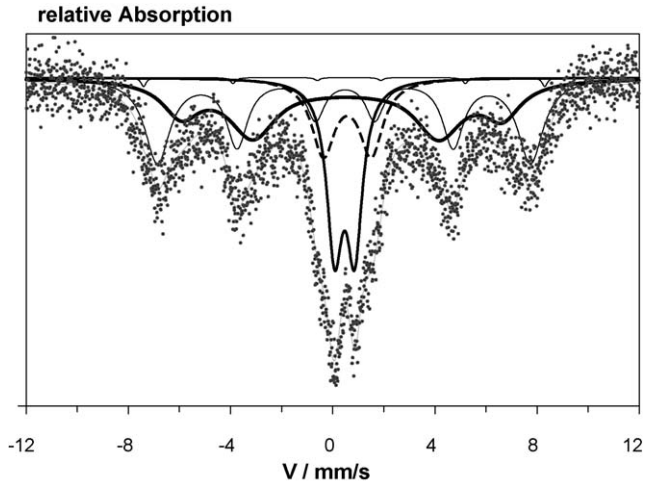

Fig. 3. ^{57}Fe Mössbauer spectrum of the 1Fe/HBEA zeolite catalyst recorded at 20 °C. The diagram includes the sub-bands obtained by deconvolution (black curves) as well as the trace arising from addition of these sub-bands (grey curve).

magnetically ordered structures. However, the unambiguous assignment to defined compounds is difficult, since the Fe entities are nano-ranged with a maximum size of about 5 nm as proven by HRTEM. Contrary, the Mössbauer data listed in the literature refer to crystalline bulk samples [26] and therefore these references have to be considered with caution. The Mössbauer spectrum of α-Fe_2O_3 recorded for comparison purposes (−196 °C) showed the expected sextet pattern including an isomer shift of 0.47 mm/s, quadrupole splitting of 0.39 mm/s and magnetic hyperfine field of 54.0 T [26]. Although the isomeric shifts of the sextet sub-bands resemble that of the reference, their quadrupole splits are much too small to be related to α-Fe_2O_3 being thermodynamically favoured. A careful comparison with literature data suggests that the sextet with an isomer shift of 0.47 mm/s is tentatively assigned to $Fe(OH)_3$ entities, while that with 0.44 mm/s is rather ascribable to FeO(OH) [26]. The presence of hydroxide as structural unit is assessed to be reasonable as hydroxylation by water vapour, that occurs on all oxide surfaces, should lead to significant OH content. Finally, the doublet sub-bands indicate highly dispersed Fe^{3+} species without magnetic order, i.e. paramagnetic entities [27,28].

The Mössbauer spectrum taken at room temperature (20 °C) showed a doublet profile being clearly different from that obtained at −196 °C (Fig. 3). Deconvolution provided three sub-doublets (R^2 = 0.96) with isomer shifts of 0.33, 0.34 and 0.35 mm/s and quadrupole splittings of 1.31, 0.94 and 0.59 mm/s (Table 4). These features are again ascribed to high spin Fe^{3+} sites. The disappearance of the sextet bands is associated with the superparamagnetic nature of these species implying loss of the magnetic order by thermal fluctuations, i.e. the ambient thermal energy is sufficient to change the direction of the magnetic moments. This behaviour was reported for particle sizes of a few nano-meters and below that [29] and is in line with the HRTEM images (Fig. 1). Moreover, the doublets found at 20 °C are shifted to lower isomer shifts as compared to −196 °C due to the second-order Doppler effect.

Table 4
Results of the ^{57}Fe Mössbauer spectroscopic analysis of the 1Fe/HBEA catalyst performed at 20 °C.

Signal[a]	Isomer shift (mm/s)	Quadrupole split (mm/s)	Fraction (%)
Doublet	0.33	1.31	21
Doublet	0.34	0.94	29
Doublet	0.35	0.59	50

[a] Signals were obtained by deconvolution of the recorded spectrum; R^2 is 0.95.

When comparing the UV–vis and Mössbauer spectroscopic results it has to be pointed out that the respective sub-bands were not obtained based on a detailed physico-chemical model and particularly for UV–vis the classification of the three different types of Fe species is rather rough. Despite this, a quantitative correlation of both spectroscopic tools is carefully attempted. The Mössbauer sextet signals refer to superparamagnetic entities with a relative abundance of ca. 68%. These components show a maximum size of about 5 nm and are obviously assigned to particulate species classified by UV–vis. However, as UV–vis indicates only a fraction of ca. 16% for these strongly aggregated species, it may be derived that the majority of the oligomeric structures is superparamagnetic as well. Oligomeric and particulate sites together reveal a proportion of 75% which is close to that found for the superparamagnetic entities (68%). Additionally, since the highly dispersed Fe sites identified by UV–vis exclude significant magnetic order, these species be ascribed to the Mössbauer doublets. This interpretation is supported by the similar fractions estimated by both spectroscopic methods, i.e. 25 and 33%.

3.2. SCR performance of the 1Fe/HBEA catalyst

The SCR performance of granulated 1Fe/HBEA and $V_2O_5/WO_3/TiO_2$ both investigated in the simple model exhaust is shown in Fig. 4. These data evidence higher SCR activity of 1Fe/HBEA below 300 °C being crucial for diesel engines. This superiority is also reflected by the apparent turnover frequency (TOF) representing the molar number of NO_x which is converted per total number of Fe (or V) and time. For example, at 200 °C the apparent TOF of 1Fe/HBEA is 8.5×10^{-3}/s, whereas for $V_2O_5/WO_3/TiO_2$ it is 1.0×10^{-3}/s; note that the apparent TOF implies that some V sites of the homogenous catalyst might be inaccessible to the feed. This global comparison shows higher activity of the Fe sites as compared to the V species. However, above 300 °C the $V_2O_5/WO_3/TiO_2$ catalyst revealed higher NO_x conversions due to restriction of SCR by NH_3 oxidation on 1Fe/HBEA. This feature is substantiated by our previous work [19] evidencing strong catalytic NH_3/O_2 reaction above 300 °C. Additionally, below 300 °C 1Fe/HBEA showed minor difference between NO_x and NH_3 conversion which we had recently attributed to NO_2-SCR side reaction including a NO_2/NH_3 stoichiometry of 0.75; NO oxidation on 1Fe/HBEA started at 150 °C leading to a NO_2 yield of 25% at 200 °C and 40% at 250 °C. Contrary, $V_2O_5/WO_3/TiO_2$ exhibited stoichiometric conversion of NO and

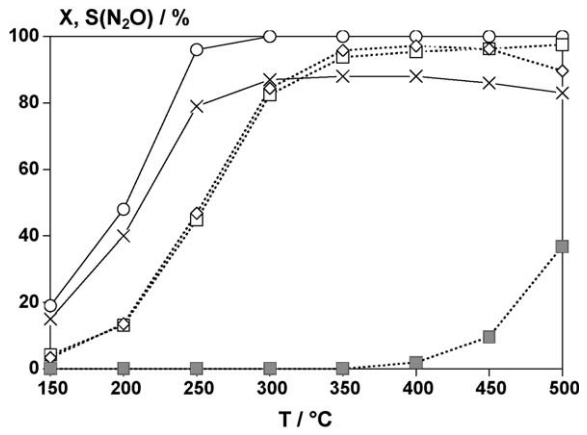

Fig. 4. SCR performance of the granulated catalysts 1Fe/HBEA (X(NO_x) ×, X(NH_3) ○) and $V_2O_5/WO_3/TiO_2$ (X(NO_x) ◇, X(NH_3) □, S(N_2O) ■). Conditions: m = 200 mg, c(NO) = 500 ppm, c(NH_3) = 500 ppm, c(O_2) = 5 vol.%, N_2 balance, S.V. = 50,000/h.

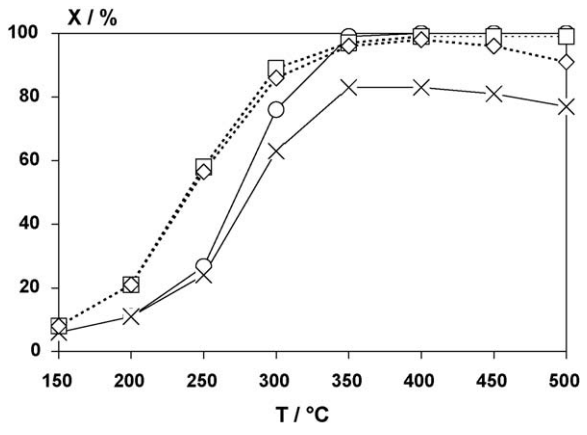

Fig. 6. SCR performance of the honeycomb coated by 1Fe/HBEA (X(NO_x) ×, X(NH_3) ○) and the homogeneous $V_2O_5/WO_3/TiO_2$ honeycomb (X(NO_x) ◇, X(NH_3) □). Conditions: c(NO) = 500 ppm, c(NH_3) = 500 ppm, c(CO) = 1000 ppm, c(O_2) = 5 vol.%, c(H_2O) = 4 vol.%, c(CO_2) = 4 vol.%, N_2 balance, S.V. = 35,000/h; load of 1Fe/HBEA was 82 g/l.

NH_3 in the entire temperature regime according to the standard SCR route. A slight discrepancy was observed at 450 and 500 °C, where N_2O formed with a selectivity of 10 and 37%, respectively. This production of N_2O is associated with the thermal dehydroxylation of reactive V(OH) groups, but is completely suppressed in presence of H_2O due to rehydration effects [30] as shown below. Unlike that, 1Fe/HBEA indicated no evolution of nitrous oxide in the whole temperature range.

The evaluation of 1Fe/HBEA granules in a more realistic feed (Fig. 5), i.e. in presence of CO, CO_2 and H_2O, resulted in decrease in deNO_x particularly at 200 and 250 °C. This decline is also reflected by the apparent TOF. For instance at 200 °C, the apparent TOF amounts to 8.5×10^{-3}/s in the simple feed, whereas with CO, CO_2 and H_2O it is reduced to 6.5×10^{-3}/s. As deduced from a related Fe/HBEA catalyst revealing a Fe content of 0.25 wt.% [18], the decrease in SCR is mainly referred to the competitive adsorption of H_2O on catalytically active sites, while CO and CO_2 do not affect the performance significantly. Nevertheless, very similar SCR data were obtained in simple and realistic feed above 300 °C. This suggests that the deactivating effect of H_2O is over-compensated at elevated temperature.

The SCR performance of the 1Fe/HBEA catalyst coated on the lab-scale honeycomb was studied with the practical feed (Fig. 6). The reaction conditions were very similar to the granulated samples except for the ratio of sample weight to flow which was almost three times higher for the granules (24×10^{-3} gs/cm^3) as compared to the honeycomb coating (9.0×10^{-3} gs/cm^3). Thus, it is not surprising that the honeycomb system provided declined NO_x conversions, particularly below 350 °C. Furthermore, above 300 °C the different conversions of NO_x and NH_3 were observed relating to NH_3 oxidation as discussed above. Contrary, the homogenous $V_2O_5/WO_3/TiO_2$ honeycomb showed significantly higher NO_x conversions below 350 °C including standard SCR stoichiometry. However, the homogenous honeycomb implies relatively high mass of V thus leading to a lower apparent TOF value, e.g. at 200 °C TOF is 0.58×10^{-3}/s, while for the honeycomb with 1Fe/HBEA coating it is 1.3×10^{-3}/s.

Nevertheless, when establishing a NO_2/NO_x ratio of 0.5 both honeycomb samples showed remarkable NO_x conversions in the low temperature region relating to the fast SCR reaction (Fig. 7), whereas 1Fe/HBEA and $V_2O_5/WO_3/TiO_2$ revealed very similar performance. Additionally, almost complete NO_x conversion was observed between 250 and 400 °C indicating that fast SCR suppresses NH_3 oxidation on 1Fe/HBEA.

The results of the engine bench tests are shown in Fig. 8 indicating similar deNO_x activity of the honeycombs coated by 1Fe/HBEA and $V_2O_5/WO_3/TiO_2$. Interestingly, high performance was already observed in the low temperature range (<225 °C)

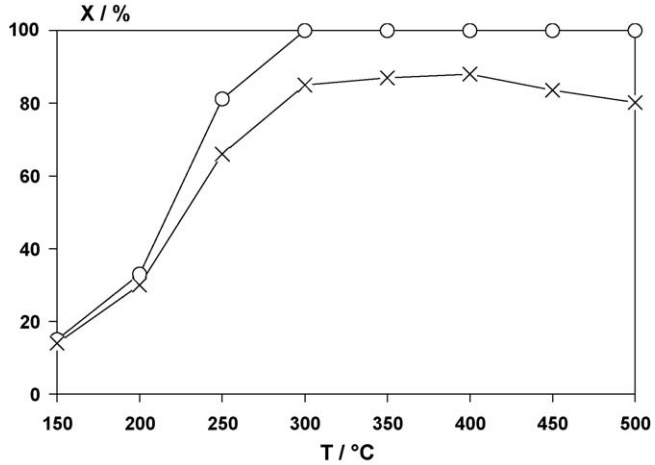

Fig. 5. SCR performance of granulated 1Fe/HBEA catalyst in practical feed (X(NO_x) ×, X(NH_3) ○). Conditions: c(NO) = 500 ppm, c(NH_3) = 500 ppm, c(CO) = 1000 ppm, c(O_2) = 5 vol.%, c(H_2O) = 5 vol.%, c(CO_2) = 5 vol.%, N_2 balance, S.V. = 50,000/h.

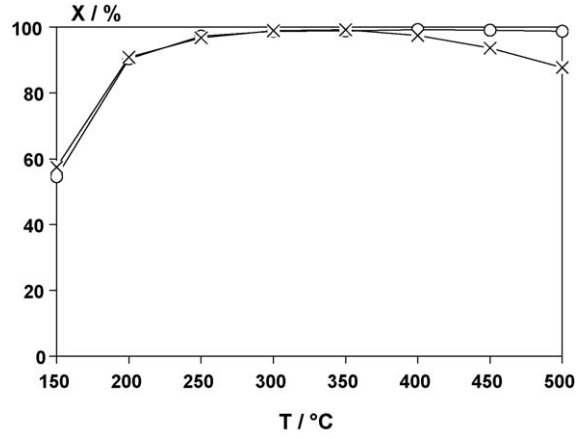

Fig. 7. SCR performance of the honeycomb coated by 1Fe/HBEA (X(NO_x) ×, X(NH_3) ○) at a molar NO_2/NO_x ratio of 0.5. Conditions: c(NO) = 250 ppm, c(NO_2) = 250 ppm, c(NH_3) = 500 ppm, c(CO) = 1000 ppm, c(O_2) = 5 vol.%, c(H_2O) = 4 vol.%, c(CO_2) = 4 vol.%, N_2 balance, S.V. = 35,000/h; load of 1Fe/HBEA was 82 g/l.

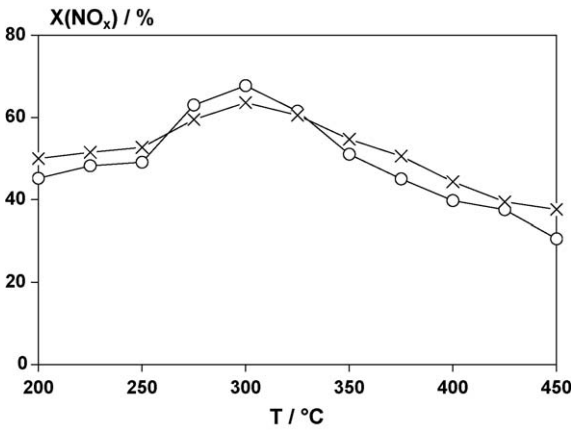

Fig. 8. NO_x conversion of the honeycomb coated by 1Fe/HBEA (×) and $V_2O_5/WO_3/TiO_2$ (○) on the engine test bench. Conditions are listed in Tables 1 and 2; load of 1Fe/HBEA was 95 g/l.

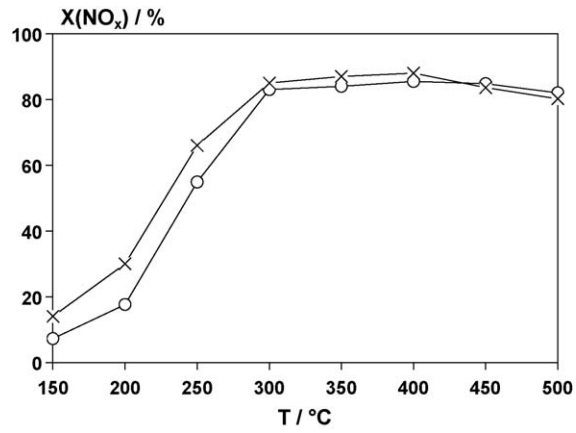

Fig. 9. NO_x conversion of fresh (×) and hydrothermally aged 1Fe/HBEA granules (○) in practical feed. Conditions: c(NO) = 500 ppm, $c(NH_3)$ = 500 ppm, c(CO) = 1000 ppm, $c(O_2)$ = 5 vol.%, $c(H_2O)$ = 5 vol.%, $c(CO_2)$ = 5 vol.%, N_2 balance, S.V. = 50,000/h. Hydrothermal aging was made at 550 °C for 24 h with 10 vol.% H_2O and 16 vol.% O_2.

with growing deNO_x up to 300 °C. This feature is associated with the increasing proportion of NO_2, i.e. fast SCR. At 200 °C the NO_2 yield of DOC was ca. 15%, while at 300 °C it was approx. 45%. However, above 300 °C the NO_x conversion decreased being referred to the space velocity mounting up to approx. 71,000/h. No N_2O was formed on both catalysts in the entire temperature range.

3.3. Stability of the 1Fe/HBEA catalyst

The hydrothermal aging of 1Fe/HBEA granules conducted for 24 h at 550 °C caused a slight decline in deNO_x at low temperatures when using the practical feed. But, above 300 °C the same performance was achieved as for the fresh catalyst (Fig. 9). This indicates compensation of the reduced performance by increased

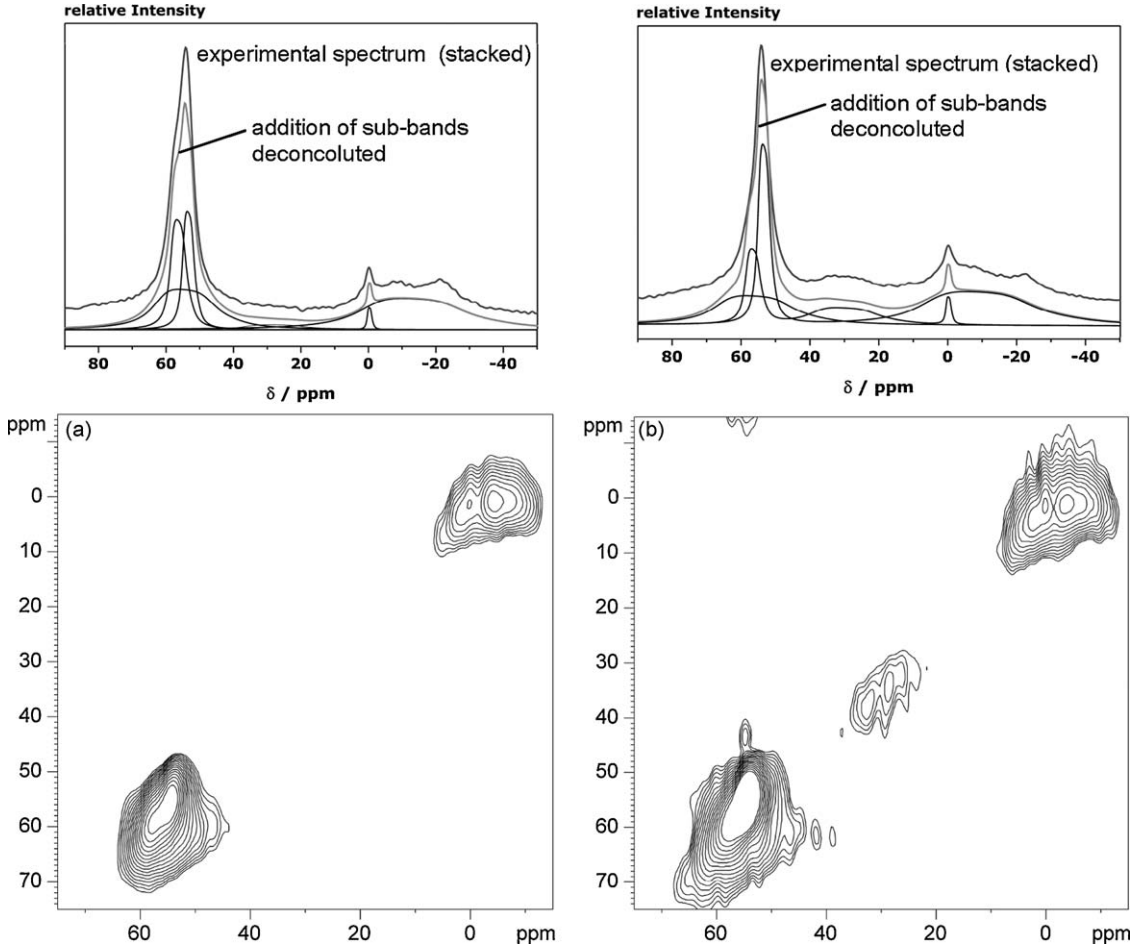

Fig. 10. ^{27}Al MQ MAS NMR spectrum of fresh (a) and hydrothermally aged 1Fe/HBEA catalyst (b). Corresponding ^{27}Al MAS NMR spectrum is on top including the experimental data, sub-bands obtained from deconvolution as well as addition of these sub-bands. Hydrothermal aging was made at 550 °C for 24 h with 10 vol.% H_2O and 16 vol.% O_2.

Table 5
Results of the ^{27}Al (MQ) MAS NMR analysis of fresh and hydrothermally aged 1Fe/HBEA catalyst[a]: chemical shift (δ), quadrupolar coupling constant (QCC) and fraction (y) of the specific Al species.[b].

	$Al(IV)_a$	$Al(IV)_b$	$Al(IV)_c$	Al(V)	$Al(VI)_a$	$Al(VI)_b$
Fresh						
δ (ppm)	59.1	55.4	59.1	30.5	0.5	1.5
QCC (MHz)	2.8	2.4	5.5	5.5	1.5	7.2
y (%)	22	18	26	3	4	27
Aged						
δ (ppm)	59.0	55.3	59.1	30.5	0.5	1.5
QCC (MHz)	2.7	2.4	5.8	5.8	1.6	7.4
y (%)	8	19	25	15	5	28

[a] Conditions of hydrothermal aging: 24 h at 550 °C with 10 vol.% H_2O and 16 vol.% O_2.
[b] The specific Al species were obtained by deconvoluting corresponding ^{27}Al MQ MAS NMR spectrum (cf. Fig. 10); for both spectra R^2 is 0.97.

temperatures. Moreover, the aging showed no impact on the fast SCR activity. When a $c(NO_2)/c(NO_x)$ ratio of 0.50 was adjusted the same efficiency was observed as for the fresh sample. Thus, these results indicate high hydrothermal stability of 1Fe/HBEA for heavy duty diesel applications. It is clear that the maximum temperatures of heavy duty vehicles are less pronounced as compared to passenger cars providing temperatures up to ca. 800 °C in DPF regeneration. It is expected that 800 °C aging of 1Fe/HBEA leads to strong decrease in $deNO_x$ as shown recently for a related Fe/HBEA sample [18].

The 1Fe/HBEA catalyst hydrothermally aged at 550 °C was characterised by UV–vis, PXRD, ^{27}Al (MQ) MAS NMR, BET and NH_3-TPD examinations. The UV–vis spectrum provided no significant difference between the fresh and aged catalyst. Both samples showed the same relative abundance of highly dispersed, oligomeric and particulate Fe species as mentioned in Section 3.1. From these results it is inferred that the hydrothermal aging does not significantly affect the structure of the Fe sites. Furthermore, same PXRD patterns were obtained for the fresh and aged catalyst, while only a slight decline in the BET surface (ca. 5%) and in the NH_3 uptake at 250 °C (fresh: 100 μmol/g ± 10%, aged: 80 μmol/g ± 10%) was observed [31].

The ^{27}Al MQ MAS NMR spectrum of fresh 1Fe/HBEA displayed resonances in the region of 50–60 ppm and around ca. 0 ppm being assigned to tetrahedral and octahedral Al sites (Fig. 10a). Spectral deconvolution was performed with a minimum set of Lorentz curves (R^2 = 0.97) [32] leading to six sub-signals (Table 5). The deconvolution shows the three different types of tetrahedral Al sites of the BEA zeolite as known from the literature, i.e. $Al(IV)_a$, $Al(IV)_b$ and $Al(IV)_c$ [33]. $Al(IV)_a$ and $Al(IV)_b$ are associated with the BEA framework, while $Al(IV)_c$, which is characterised by larger quadrupolar interactions derived from the broadening parallel to the F2 axis, exists in extra-framework positions [34]. The obtained octahedral sites $Al(VI)_a$ and $Al(VI)_b$ are also related to extra-framework species; octahedral Al centres accommodated by the zeolite structure would appear as a rather sharp peak with minor quadrupolar coupling and narrow chemical shift distribution. Furthermore, a extra-framework penta-coordinated Al(V) sites are detected in negligible amounts only. Table 5 shows that about 60% of the Al sites are not in framework positions being in line with findings from Beers et al.; these species might be left over from the synthesis or some dealumination might have been occurred in the post-synthesis treatment [33].

After the hydrothermal exposure of 1Fe/HBEA an increased fraction of Al(V) and changes in the peak intensities of Al(IV) species were noticed (Fig. 10b). Within the accuracy of the analyses, the $Al(IV)_a/Al(IV)_b$ ratio decreases from 1.2 for the fresh sample to 0.42 for the aged one (Table 5). This indicates substantial reduction of the framework $Al(IV)_a$ sites, whereas the relative proportion of the extra-framework $Al(IV)_c$ is maintained. Additionally, the respective amounts of the octahedral Al sites do not change significantly.

Combining the PXRD and ^{27}Al MAS NMR results it is evident that the conversion of framework into extra-framework sites occurring in the hydrothermal aging does not significantly affect the stability of the BEA zeolite structure. This is in accordance with Beers et al. investigating the hydrothermal resistance of BEA zeolite under similar conditions [33]. It may be speculated that the loss of the $Al(IV)_a$ species contributes to the slight decrease in NH_3 uptake. It is known that the number of framework Al sites accounts for the amount of the Bronsted OH groups [35] which are involved in the NH_3 adsorption [31].

The interaction of 1Fe/HBEA with SO_2 was elucidated by DRIFT spectroscopy providing very similar spectra irrespective of the admitted gas mixture (SO_2/N_2, SO_2/O_2) and temperature (50, 300 °C). Fig. 11 exemplarily demonstrates the data recorded after exposure to SO_2/N_2 for 48 h at 300 °C and subsequent flushing with N_2; purging did not influence the shape of the spectrum. The DRIFT spectrum revealed broad bands at ca. 1190 and 1350 cm^{-1} which refer to the ν_s and ν_{as} vibrations of adsorbed SO_2 [36]. These frequencies are very close to gaseous SO_2 (1151 and 1362 cm^{-1}) evidencing rather weak bond to the catalyst surface. Since the same features were observed with bare H-BEA, it is obvious that SO_2 is predominately adsorbed on the substrate. In accordance with the literature [36,37] the uptake of SO_2 is assumed to occur on both O^{2-} framework sites and OH groups. The interaction with the latter is indicated by slight perturbation of the broad OH stretching band between 3350 and 3670 cm^{-1} (not depicted). But, no sulphite and sulphate species were observed for 1Fe/HBEA which might be assigned to the interaction of Fe sites with SO_2 and SO_3,

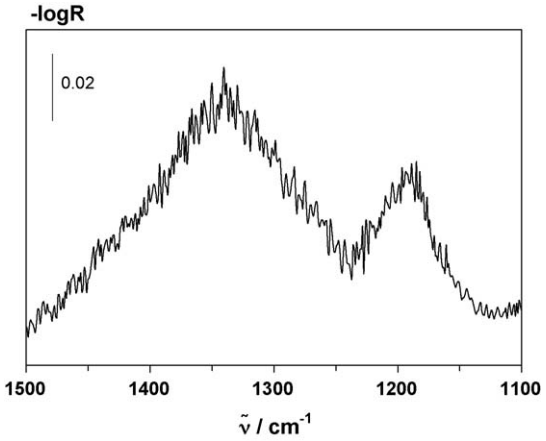

Fig. 11. DRIFT spectrum of 1Fe/HBEA catalyst after exposure to 20 ppm SO_2 in N_2 at 300 °C and subsequent flushing in N_2; sample was pre-treated in N_2 at 500 °C for 15 min.

respectively [36,38]. The absence of sulphate shows low SO_2 oxidation activity of the catalyst. Furthermore, when the sample was exposed to SO_2 at 50 °C and was then heated in N_2 to 400 °C the bands at 1190 and 1350 cm^{-1} disappeared completely substantiating the release of the SO_2. For practice, this relatively low thermal stability of the adsorbed SO_2 species is advantageous as possible regeneration of the catalyst can be simply achieved by extra urban driving providing temperatures above 400 °C. Due to this finding the SCR study of 1Fe/HBEA aged for 48 h with SO_2/O_2 was started at 300 °C and then temperature was decreased to 150 °C thus avoiding desorption of SO_2. The results of this run showed same deNO_x as for the fresh catalyst thus excluding susceptibility of 1Fe/HBEA to SO_2 poisoning. The SCR measurement was made by employing the simple model exhaust.

4. Conclusions

This paper deals with SCR to remove NO_x from heavy duty vehicles employing the highly efficient 1Fe/HBEA zeolite catalyst. The catalytic studies showed higher efficiency of 1Fe/HBEA granules as compared to traditional $V_2O_5/WO_3/WO_3$. This is substantiated by the apparent turnover frequency showing pronounced activity of the Fe sites referred to vanadium. Additionally, no formation of N_2O was observed indicating selective NO_x reduction into N_2. In accordance with recent results, the high activity of 1Fe/HBEA is closely related to the prominent presence of highly dispersed and oligomeric Fe oxo species. The former entities are supposed to be paramagnetic, while the latter are superparamagnetic. Strongly aggregated structures being less active show superparamagnetic behaviour as well.

Furthermore, a honeycomb prototype coated by 1Fe/HBEA was prepared and compared to a commercial $V_2O_5/WO_3/TiO_2$ sample. Although the honeycomb with 1Fe/HBEA showed high activity and its apparent turnover frequency is superior, the $V_2O_5/WO_3/TiO_2$ sample revealed higher NO_x conversion under standard SCR conditions, particularly in the low temperature range. This discrepancy evidences the potential to optimise the preparation of the honeycomb system. However, under fast SCR conditions 1Fe/HBEA and $V_2O_5/WO_3/TiO_2$ honeycombs showed same performance including considerable deNO_x at low-temperatures. This finding was confirmed by the engine bench tests proving the capability of 1Fe/HBEA to substitute vanadia based catalysts. Finally, hydrothermal aging specifically performed for heavy duty applications as well as SO_2 aging indicate high stability of 1Fe/HBEA. Thus, the 1Fe/HBEA catalyst shows encouraging potential for further optimisation steps to meet future exhaust limits of heavy duty vehicles without need of $V_2O_5/WO_3/TiO_2$ catalysts.

Acknowledgement

The authors would like to acknowledge the German Foundation of Environment (Deutsche Bundesstiftung Umwelt) for partially financing this work under the project AZ 23251.

References

[1] F.J. Janssen,, in: G. Ertl, H. Knözinger, J. Weitkamp (Eds.), 1st edition, Handbook of Heterogeneous Catalysis, vol. 4, VCH Wiley, Weinheim, 1997, p. 1633.
[2] A. Grossale, I. Nova, E. Tronconi, D. Chatterjee, M. Weibel, J. Catal. 256 (2008) 312.
[3] M. Devadas, O. Kröcher, M. Elsener, A. Wokaun, N. Söger, M. Pfeifer, Y. Demel, L. Mussmann, Appl. Catal. B 67 (2006) 187.
[4] O. Salvat, P. Marez, G. Belot, SAE Paper 2000-01-0473.
[5] B.J. Cooper, J.E. Thoss, SAE Paper 890404.
[6] K.M. Santhosh, M. Schwidder, W. Grünert, A. Brückner, J. Catal. 227 (2004) 384.
[7] M. Schwidder, K.M. Santhosh, A. Brückner, W. Grünert, Chem. Commun. 6 (2005) 805.
[8] M. Schwidder, K.M. Santhosh, K. Klementiev, M. Marga, A. Brückner, W. Grünert, J. Catal. 231 (2005) 314.
[9] R.Q. Long, R.T. Yang, J. Catal. 188 (1999) 332.
[10] R.Q. Long, R.T. Yang, Catal. Lett. 74 (2001) 201.
[11] Q. Sun, Z.X. Gao, H.Y. Chen, W.M.H. Sachtler, J. Catal. 201 (2001) 89.
[12] H.Y. Chen, Q. Sun, B. Wen, Y.H. Yeom, E. Weitz, W.M.H. Sachtler, Catal. Today 96 (2004) 1.
[13] Q. Sun, Z.X. Gao, B. Wen, W.M.H. Sachtler, Catal. Lett. 78 (2002) 1.
[14] G. Qi, R.T. Yang, Appl. Catal. B 60 (2005) 13.
[15] H. Sjövall, L. Olsson, E. Fridell, R.J. Blint, Appl. Catal. B 64 (2006) 180.
[16] Y. Li, H. Cheng, D. Li, Y. Qin, Y. Xie, S. Wang, Chem. Commun. (2008) 1470.
[17] S. Djerad, B. Geiger, F.J.P. Schott, S. Kureti, Catal. Commun. 20 (2009) 1103.
[18] P. Balle, B. Geiger, S. Kureti, Appl. Catal. B 85 (2009) 109.
[19] D. Reichert, H. Bockhorn, S. Kureti, Appl. Catal. B 84 (2008) 803.
[20] J.P. Amoureux, C. Fernandez, S. Steuernagel, J. Magn. Reson. A 123 (1996) 116.
[21] D.J. States, R.A. Haberkorn, D.J. Ruben, J. Magn. Reson. 48 (1982) 286.
[22] M. Müller, G. Harvey, R. Prins, Micropor. Mesopor. Mater. 34 (2000) 135.
[23] J.A. van Bokhoven, D.C. Konigsberger, P. Kunkeler, H. van Bekkum, A.P.M. Kentgens, J. Am. Chem. Soc. 122 (2000) 12842.
[24] E. Murad, J. Cashion, Mössbauer Spectroscopy of Environmental Materials and Their Industrial Utilization, Kluwer, 2003.
[25] D.M. Sherman, Phys. Chem. Miner. 12 (1985) 161.
[26] S.J. Oh, D.C. Cook, H.E. Townsend, Hyperfine Interact 112 (1998) 59.
[27] Y. Okamoto, T. Kubota, Y. Ohto, S. Nasu, J. Catal. 192 (2000) 412.
[28] M. Iwasaki, K. Yamazaki, K. Banno, H. Shinjoh, J. Catal. 260 (2008) 205.
[29] R.M. Cornell, U. Schwertmann, The Iron Oxides, 2nd edition, Wiley-VCH Weinheim, 2003.
[30] A. Burkardt, W. Weisweiler, J.A.A. van den Tillaart, A. Schafer-Sindlinger, E.S. Lox, Top. Catal. 16 (2001) 369.
[31] D. Klukowski, P. Balle, B. Geiger, S. Wagloehner, S. Kureti, B. Kimmerle, A. Baiker, J.-D. Grunwaldt, submitted for publication.
[32] D. Massiot, F. Fayon, M. Capron, I. King, S. Calvé, B. Alonso, J.-O. Durand, B. Bujoli, Z. Gan, G. Hoatson, Magn. Reson. Chem. 40 (2002) 70.
[33] A.E.W. Beers, J.A. van Bokhoven, K.M. de lathouder, F. Kapteijn, J.A. Moulijn, J. Catal. 218 (2003) 239.
[34] J.M. Newsam, M.M.J. Treacy, W.T. Koetsier, C.B. deGruyter, Proc. R. Soc. London A 420 (1988) 375.
[35] A. Corma, Chem. Rev. 95 (1995) 559.
[36] A. Davydov, Molecular Spectroscopy of Oxide Catalyst Surfaces, John Wiley, Chichester, 2003.
[37] H.G. Karge, I.D. Lana, J. Phys. Chem. 88 (1984) 1538.
[38] A. Kaya, T. Yamaguchi, K. Tanabe, J. Catal. 83 (1983) 99.